Evolution of anisotropic in-plane resistivity with doping level in $Ca_{1-x}Na_xFe_2As_2$ single crystals

J. Q. Ma,[1] X. G. Luo,[1,2,*] P. Cheng,[1] N. Zhu,[1] D. Y. Liu,[3] F. Chen,[1,2] J. J. Ying,[1] A. F. Wang,[1] X. F. Lu,[1] B. Lei,[1] and X. H. Chen[1,†]

[1]*Hefei National Laboratory for Physical Science at Microscale and Department of Physics, University of Science and Technology of China, Hefei, Anhui 230026, People's Republic of China*

[2]*Synergetic Innovation Center of Quantum Information & Quantum Physics, University of Science and Technology of China, Hefei, Anhui 230026, China*

[3]*Key Laboratory of Materials Physics, Institute of Solid State Physics, Chinese Academy of Sciences, P.O. Box 1129, Hefei 230031, People's Republic of China*

(Received 2 April 2014; revised manuscript received 19 April 2014; published 21 May 2014)

We measured the in-plane resistivity anisotropy in the underdoped $Ca_{1-x}Na_xFe_2As_2$ single crystals. The anisotropy (indicated by $\rho_b - \rho_a$) appears below a temperature well above magnetic transition temperature T_N, being positive ($\rho_b - \rho_a > 0$) as $x \leqslant 0.14$. With increasing the doping level to $x = 0.19$, an intersection between ρ_b and ρ_a is observed upon cooling, with $\rho_b - \rho_a < 0$ at low temperature deep inside a magnetically ordered state, while $\rho_b - \rho_a > 0$ at high temperature. Subsequently, further increase of hole concentration leads to a negative anisotropy $\rho_b - \rho_a < 0$ in the whole temperature range. These results manifest that the anisotropic behavior of resistivity in the magnetically ordered state depends strongly on the competition of the contributions from different mechanisms, and the competition between the two contributions results in a complicated evolution of the anisotropy of in-plane resistivity with doping level.

DOI: 10.1103/PhysRevB.89.174512 PACS number(s): 74.25.F−, 74.62.Dh, 74.70.Xa

I. INTRODUCTION

The undoped and underdoped iron pnictides undergo structural transition upon cooling, accompanied with a magnetic transition from high-temperature paramagnetic to low-temperature antiferromagnetic (AFM) phase [1]. Understanding the origin of superconductivity in iron pnictide might start from the normal-state physics, especially the roles of the various degrees of freedom in the magnetic state. One central topic concerning these is the electronic anisotropy at low temperature, which involves the fluctuation or ordering of spin, orbital, and band structures [2–4]. In such an anisotropic electronic state, the striking behavior is that the resistivity along the ferromagnetically ordered and shorter *b* axis is larger than that along the antiferromagnetically ordered and longer *a* axis ($\rho_b - \rho_a > 0$). The anisotropy actually appears well above the structural and magnetic transition temperatures T_s and T_N in electron-underdoped Ba-122 [2,5,6], which has been discussed according to the nematicity [7–9] by considering the anisotropic magnetic scattering induced by nematic (spin or/and orbital) fluctuation. The observation of an orbital ordered polarization of d_{xz} and d_{yx} of Fe in angle-resolved photoemission spectroscopy (ARPES) [10], local anisotropies in scanning tunneling spectroscopy [11,12], anisotropies in the optical spectrum [13], and magnetic susceptibility [14] seems to support the point of view of nematicity.

However, the origin for the anisotropic in-plane resistivity in the AFM state remains in hot debate. In undoped $BaFe_2As_2$, the anisotropy has been discussed [3,15] in terms of the high-mobility Dirac pockets near the Fermi energy, detected by quantum oscillations and ARPES measurements [16–19]. Orbital ordering was also considered as a possible mechanism for the anisotropy, but calculations based on five-orbital model gave rise to a sign opposite to that observed in experiments [20,21]. Another scenario was proposed based on impurity scattering to interpret such anisotropic in-plane resistivity [6,22,23]. Especially, annealing can lead to almost annihilation of transport anisotropy at low temperature in undoped $BaFe_2As_2$ [22,23], which strongly suggests the origin from magnetic scattering of the impurity states. The very tiny anisotropy in underdoped $Ba_{1-x}K_xFe_2As_2$ was thought to be ascribed to the relatively small impurity potential as the dopant atom is relatively far from the Fe plane [6].

Very recently, it was surprisingly found in $Ba_{1-x}K_xFe_2As_2$ that, in contrast to the small positive anisotropy of resistivity ($\rho_b - \rho_a > 0$) existing at $x \leqslant 0.202$, the sign of the anisotropy was reversed to negative ($\rho_b - \rho_a < 0$) as $x = 0.235$, which begins at a temperature well above T_N [24]. However, as mentioned above, different mechanisms were considered to interpret the anisotropy above and below T_N, respectively. As a consequence, there is a natural question about how the sign of anisotropy evolves from totally positive to totally negative with increasing the hole doping level. In this paper, we report on anisotropic in-plane resistivity on detwinned hole-underdoped $Ca_{1-x}Na_xFe_2As_2$ crystals. $\rho_b - \rho_a > 0$ is observed in the samples with $x = 0.11$ and 0.14. In the sample with $x = 0.19$, however, an intersection happens at a certain temperature of 110 K in $\rho_b \sim T$ and $\rho_a \sim T$ curves; that is, $\rho_b - \rho_a < 0$ below 110 K, while $\rho_b - \rho_a > 0$ above 110 K and the sign of resistivity anisotropy is the same as that observed in the crystals with $x = 0.11$ and 0.14. Subsequently, as x is increased further ($x \geqslant 0.24$), the sign of this anisotropy can be totally reversed, $\rho_b - \rho_a < 0$, similar to the results observed in $Ba_{1-x}K_xFe_2As_2$ ($x = 0.235$). Such complicated evolution of anisotropy can be understood in terms of combined effect of spin fluctuation and the reconstructed Fermi surface (RFS) on anisotropy, with the effect of impurities included.

*Corresponding author: xgluo@ustc.edu.cn
†Corresponding author: chenxh@ustc.edu.cn

II. EXPERIMENTAL DETAILS

High-quality single crystals of $Ca_{1-x}Na_xFe_2As_2$ were grown by the self-flux method. The starting materials were CaAs, NaAs, FeAs, and Fe_2As, with the molar ratio of Ca/Na : Fe : As = 1 : 4 : 4. The nominal compositions were $x = 0.2, 0.23, 0.3, 0.35$, and 0.4, respectively. After thoroughly grounding, the mixture was loaded into an alumina crucible and then sealed in an iron crucible under 1.5 atm argon atmosphere. The reactants were heated to 1160 °C in a tube furnace protected with highly pure argon and kept at this temperature for 10 h. Subsequently, the furnace was cooled down to 860 °C at a rate of 5 °C/h. Finally, the furnace was cooled down to room temperature naturally by shutting off the power. The actual chemical compositions were determined by energy dispersive x-ray spectroscopy (EDS) to be 0.11, 0.14, 0.19, 0.24, and 0.30 for the above five nominal compositions Na : Ca = 0.2–0.40, respectively, with a standard instrument error of 10%. Single-crystal x-ray diffraction (XRD) was performed on a SmartLab-9 diffractometer (Rikagu) from 10 to 65 deg with a scanning rate of 2 deg per minute. The crystals were cut in a rectangular shape along the tetragonal [110] directions. The in-plane resistivity measurements were carried out with the standard four-probe method by using a Quantum Design physical property measurement system. The in-plane resistivity along the orthorhombic *a* and *b* axes was measured by a mechanical cantilever device similar to that in Refs. [2,5].

III. RESULTS AND DISCUSSION

Figure 1(a) shows the single-crystal XRD patterns for the $Ca_{1-x}Na_xFe_2As_2$ single crystals with $x = 0.11$–0.24. Only (0 0 2*l*) reflections show up, suggesting good orientation along the c axis for all the crystals. The typical rocking curve of (0 0 2) reflection for the crystals is shown in Fig. 1(b). The full width at half maximum of the rocking curve is about 0.16 deg, indicating the high quality of the crystals. The inset of Fig. 1(b) shows lattice constant *c* estimated from the data shown in Fig. 1(a), which increases nearly linearly with increasing Na doping level, consistent with the previous report on the polycrystalline samples of $Ca_{1-x}Na_xFe_2As_2$ [25].

The temperature dependence of the in-plane resistivity measured on twinned $Ca_{1-x}Na_xFe_2As_2$ crystals ($x = 0.11$–0.30) is shown in Fig. 2. The residual resistivity decreases with increasing doping level and becomes less than 44 $\mu\Omega$ cm for $x = 0.24$, which is close to that in $Ba_{1-x}K_xFe_2As_2$ crystal with 16% doping level [6]. A clear anomaly can be observed for all of these samples in the temperature region of 148 K–170 K. Such single kink of anomaly in resistivity indicates that the AFM and structural transitions take place at the same temperature, the same as that observed in the $Ba_{1-x}K_xFe_2As_2$ system [26]. Therefore, we denote the temperature where this anomaly locates simply as T_N. The observed T_N's are much higher than those observed in polycrystalline sample for each same doping level [25]. T_N is plotted against doping level in the inset of Fig. 2. With increasing the doping level, T_N decreases quite slowly as $x \leqslant 0.24$ and then steeply as $x > 0.24$. No superconductivity can be observed above 5 K as $x \leqslant 0.24$ and the sample with $x = 0.30$ shows the superconducting transition at 20 K. The nonsuperconducting

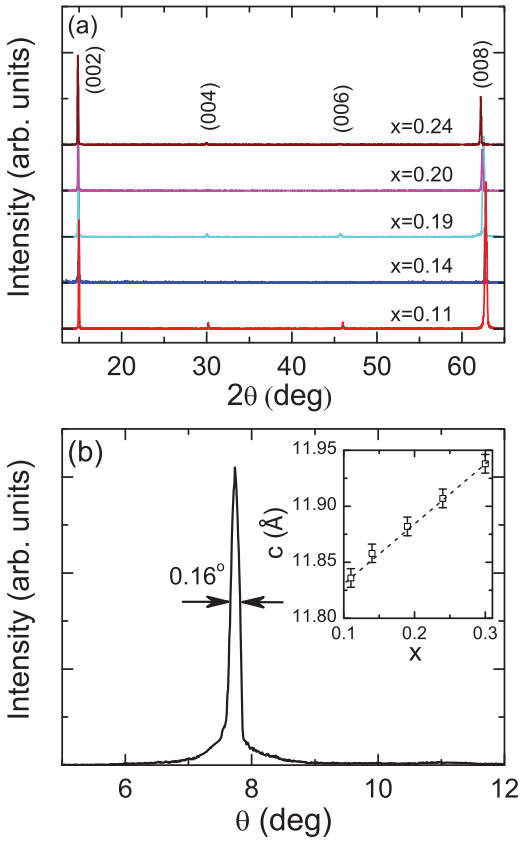

FIG. 1. (Color online) (a) The single-crystal XRD patterns for $Ca_{1-x}Na_xFe_2As_2$ single crystals with $x = 0.11$–0.24. (b) Typical rocking curve of (002) reflection. The inset shows x dependence of the lattice parameter *c* estimated from the data in (a).

underdoped region in $Ca_{1-x}Na_xFe_2As_2$ is much wider than that of $Ba_{1-x}K_xFe_2As_2$ [26], in which superconductivity emerges as $x > 0.14$.

The twin boundaries in the orthorhombic phase of the underdoped iron pnictides [27] hampers probing the in-plane anisotropy and two methods (application of uniaxial strain or

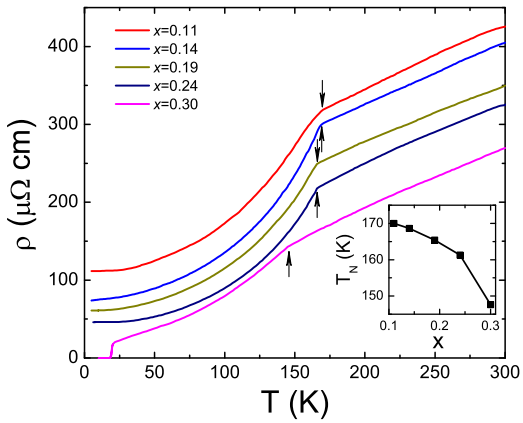

FIG. 2. (Color online) Temperature dependence of the in-plane resistivity measured on twinned $Ca_{1-x}Na_xFe_2As_2$ crystals with $x = 0.11$–0.30. The arrows indicate the magnetic transition temperatures, where the maximum of the derivative of resistivity locates. The doping dependence of AFM transition temperature T_N is shown in the inset.

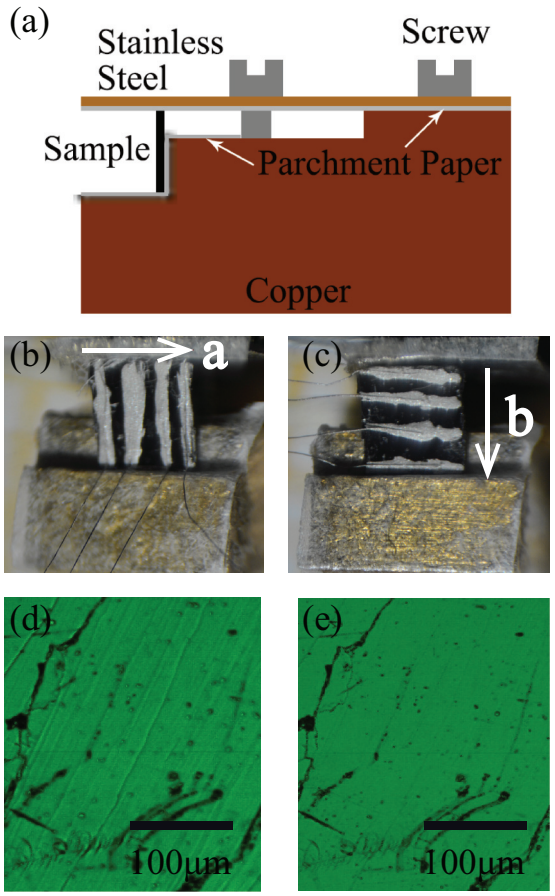

FIG. 3. (Color online) (a) The schematic view of the setup for detwinning in this work. The parchment paper is used for insulating the sample from copper substrate and the stainless steel cantilever. (b),(c) A single-crystal sample of $Ca_{1-x}Na_xFe_2As_2$, mounted on the detwinning setup with the contacts aligned parallel and perpendicular to the direction of the strain pressure. (d),(e) The polarized-light microscopic views for the surface of twinned and detwinned case taken at 77 K, respectively.

tensile and imposing an in-plane magnetic field) have been adopted to detwin such crystals so that the orthorhombic a and b axes can be distinguished [2,4,5,10,19,28,29]. In this work, uniaxial strain was used for detwinning the crystals. The setup adopted in the study of the in-plane resistivity anisotropy is schematically shown in Fig. 3(a), which has widely been used in the previous works [2,5] for detwinning iron-pnictide crystals. The mechanical strain was produced by tightening the screw nearby the sample and applied along the tetragonal [110] direction (which would become the orthorhombic a or b axis in the orthorhombic phase), as mentioned above. The typical configurations of current and voltage contacts for measuring resistivity along the orthorhombic a and b axes are shown in Fig. 3(b) and 3(c), respectively. Figures 3(d) and 3(e) are the typical polarized-light microscopy of the surface of $Ca_{0.89}Na_{0.11}Fe_2As_2$ crystal at the temperature of 77 K before and after detwinning, respectively. After detwinning, twin domain walls can no longer be seen, as shown in Fig. 3(e).

Figure 4 shows the temperature dependence of the in-plane resistivity along the a and b axes (ρ_a and ρ_b) of the detwinned $Ca_{0.89}Na_{0.11}Fe_2As_2$. Small anisotropy of in-plane resistivity

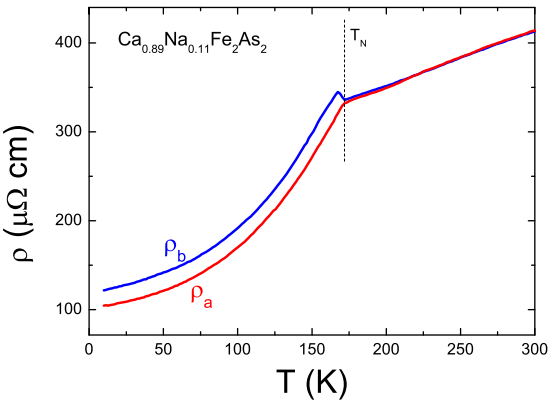

FIG. 4. (Color online) Temperature dependence of the in-plane resistivity measured on the detwinned $Ca_{0.89}Na_{0.11}Fe_2As_2$ crystal (blue, ρ_b; red, ρ_a). T_N is determined from resistivity measured on twinned crystal, as shown in Fig. 2.

can be observed well above T_N and it becomes larger as temperature is cooled close to T_N. A finite difference between ρ_a and ρ_b in the AFM state remains to low temperature. The resistivity along the b axis is larger than that along the a axis, e.g., $\rho_b > \rho_a$, which is similar to those observed in parent $CaFe_2As_2$ and other electron-doped Ba- and Eu-122 crystals [2–5].

With the increase of the Na doping level, the anisotropy becomes small, as observed for $Ca_{0.86}Na_{0.14}Fe_2As_2$ crystal [see Fig. 5(a)]. As shown in Fig. 5(c), $\rho_b < \rho_a$ can be observed below a temperature well above T_N for the crystal with $x = 0.24$, which resembles previous observation in $Ba_{1-x}K_xFe_2As_2$ with nearly the same hole doping level ($x = 0.235$) as ours [24]. In a previous report for the $Ba_{1-x}K_xFe_2As_2$ [24] system, the anisotropy changes from $\rho_b > \rho_a$ for the sample with $x = 0.202$ to $\rho_b < \rho_a$ for the sample with $x = 0.235$. It should be noted that the sign reversal of anisotropy in $Ba_{1-x}K_xFe_2As_2$ happens in the superconducting samples. While in the $Ca_{1-x}Na_xFe_2As_2$ system, $\rho_b < \rho_a$ can already be observed in the nonsuperconducting underdoped sample.

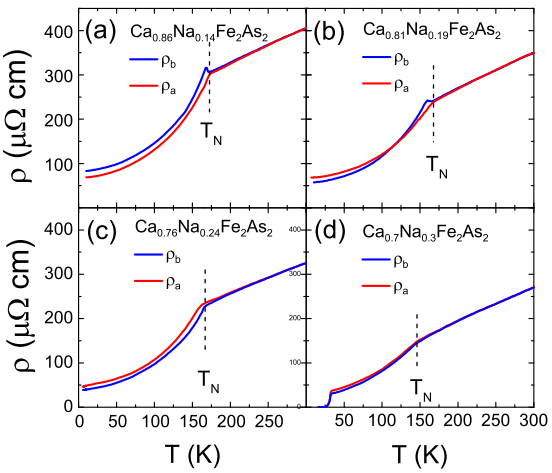

FIG. 5. (Color online) Temperature dependence of the in-plane resistivity measured on the detwinned $Ca_{1-x}Na_xFe_2As_2$ crystal (blue, ρ_a; red, ρ_b), with $x = 0.14$–0.24.

Superconductivity emerges and a small difference between ρ_b and ρ_a with $\rho_b < \rho_a$ can still be observed at low temperature for the sample with $x > 0.3$, as shown in Fig. 5(d). The onset superconducting transition temperature was enhanced by about 7 K from about 20 K at ambient pressure after applying strain pressure, indicating that superconductivity in $Ca_{1-x}Na_xFe_2As_2$ is sensitive to pressure. Although such uniaxial stress is usually low (typical values of 5–10 MPa [30]), it has been reported that superconductivity is induced by the uniaxial stress in underdoped $Ba(Fe_{1-x}Co_x)_2As_2$ with $x = 0.016$ and 0.025 [2]. Such a dramatic enhancement of T_c under small uniaxial stress applied within ab plane can be ascribed to the height of anion from the Fe atom (h) in $Ca_{0.7}Na_{0.3}Fe_2As_2$ being close to the optimal value 1.38 Å [31] (derived from the data of polycrystalline sample [25], h should be around 1.37 Å as $x = 0.3$ in $Ca_{1-x}Na_xFe_2As_2$). Uniaxial stress can reduce the lattice parameters within ab plane and consequently results in an enhancement of h. As discussed in Ref. [28], T_c can be enhanced sharply with increasing h close to 1.38 Å, and small uniaxial stress can efficiently raise T_c.

To clarify the nature of the sign reversal of in-plane resistivity anisotropy with increasing hole doping level in hole-doped iron pnictides, we studied the sample with the intermediate doping level ($x = 0.19$) to unveil how the sign of anisotropy develops with increasing the hole doping level from $x = 0.11$ and 0.14 with $\rho_b > \rho_a$ to $x = 0.24$ and 0.30 with $\rho_b < \rho_a$, as shown in Fig. 5(b). It is found that sign reversal of the anisotropy happens in the special sample with $x = 0.19$ upon cooling; that is, $\rho_b > \rho_a$ starts to be observed at a temperature well above T_N, and $\rho_a > \rho_b$ occurs below about 110 K (much less than T_N). Therefore, sign reversal of in-plane resistivity anisotropy occurs firstly at low temperature with $\rho_b > \rho_a$ at high temperature, resulting in an intersection between $\rho_a(T)$ and $\rho_b(T)$. These results suggest that there are competitive mechanisms on the anisotropy in the AFM state.

We plot the temperature dependence of the in-plane resistivity difference $\Delta\rho = \rho_b - \rho_a$ for all the samples in Fig. 6(a). The maximum of the magnitude of $\Delta\rho$ appears at temperatures a little below T_N ($T \approx 0.95T_N$) for $x = 0.11$–0.24. It is found that above T_N there is already a finite resistivity anisotropy ($\Delta\rho \neq 0$), suggesting the existence of nematic phase [7–9]. With increasing x, $\Delta\rho$ above T_N changes the sign from positive to negative at $x = 0.24$. The sign reversal of anisotropy occurs in the sample with T_N as high as 162 K, which is much higher than ~70 K in the $Ba_{1-x}K_xFe_2As_2$ case although their hole concentrations are close to each other [24]. The anisotropy of in-plane resistivity above T_N has been theoretically ascribed to the contribution from the anisotropic magnetic scattering due to the spin (nematic) fluctuations associated with the anisotropy electronic state (nematic state) [7,32], which has been proposed to explain the sign reversal in $Ba_{1-x}K_xFe_2As_2$ above T_N [7,24].

It was previously proposed that the mechanism responsible for the anisotropy below T_N should be different from that for the anisotropy above T_N due to the reconstruction of Fermi surface induced by the AFM ordering [3,20,24,30]. It has been theoretically suggested that the in-plane resistivity can be larger along either the a or the b direction, depending on the shape of the Fermi surface, because the anisotropy of the Fermi velocity (strongly connected to the morphology and topology of the RFS) can lead to a large variation in the ratio of the Drude weight along the two directions [21]. However, recent theoretical work by Sugimoto *et al.* pointed out that the Drude weight gives anisotropy opposite to experimental observation [20]. It seems to suggest that only the anisotropic RFS itself is not sufficient to interpret the observed in-plane resistivity anisotropy.

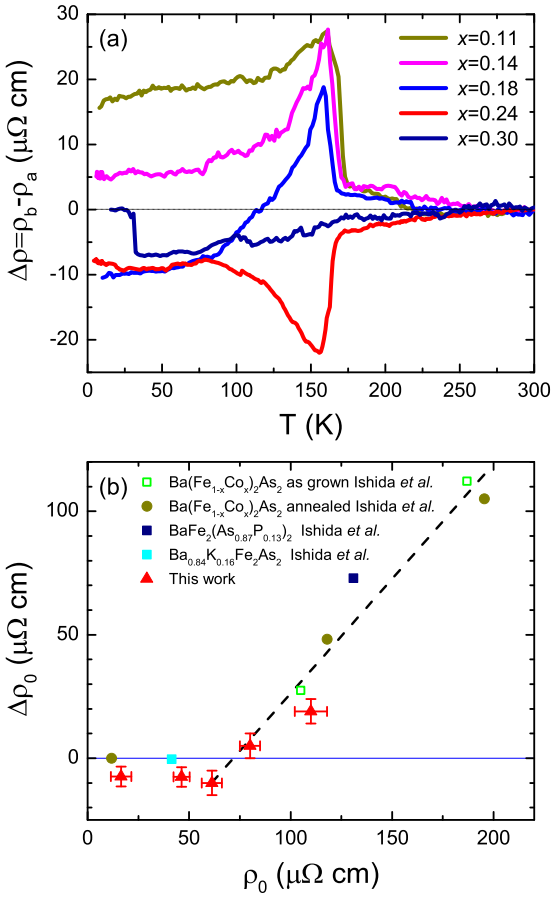

FIG. 6. (Color online) (a) Temperature dependence of the in-plane resistivity difference ($\Delta\rho = \rho_b - \rho_a$) for $Ca_{1-x}Na_xFe_2As_2$. (b) Difference in the residual component of the in-plane resistivity at low temperature plotted against the residual resistivity (ρ_0) obtained from measurements on twinned crystals (as shown Fig. 2). The data other than $Ca_{1-x}Na_xFe_2As_2$ come from Ref. [6].

The impurity scattering within the FeAs layers has also been proposed as one possible mechanism for the anisotropy of resistivity below T_N in Co- and P-doped $BaFe_2As_2$ [6,22,23]. To illustrate the effect of impurity scattering on the anisotropy in $Ca_{1-x}Na_xFe_2As_2$, we plotted the difference in the residual component of the in-plane resistivity ($\Delta\rho_0$) as a function of the residual resistivity (ρ_0) at low temperature, as shown in Fig. 6(b). The data from a previous report on Co- and P-doped $BaFe_2As_2$ are also included in Fig. 6(b) [6]. As $\Delta\rho_0 > 0$ ($x = 0.11$ and 0.14 in $Ca_{1-x}Na_xFe_2As_2$), a correlation between $\Delta\rho_0$ and ρ_0 is observed; that is, $\Delta\rho_0$ linearly decreases with reducing ρ_0. Considering that the magnitude of ρ_0 reflects the level of impurity scattering, this correlation indicates that the impurity scattering plays a significant role on the anisotropy of the in-plane resistivity, as suggested by a previous report [6].

As shown in Fig. 6(b), $\Delta\rho_0$ could reach zero as ρ_0 is reduced to about 75 $\mu\Omega$ cm. Our group and Ishida *et al.* reported a negligible $\Delta\rho_0$ in $Ba_{0.84}K_{0.16}Fe_2As_2$ which has ρ_0 ($\approx$41 $\mu\Omega$ cm) much less than 75 $\mu\Omega$ cm [5,6]. Ishida *et al.* attributed this to rather weak impurity potential [6]. However, $\Delta\rho_0$ becomes negative in $Ca_{1-x}Na_xFe_2As_2$ when ρ_0 is reduced to less than 75 $\mu\Omega$ cm with increasing Na content. A similar behavior (the finite negative $\Delta\rho_0$) has been reported in $Ba_{0.765}K_{0.235}Fe_2As_2$, which has smaller ρ_0 than that in $Ba_{0.84}K_{0.16}Fe_2As_2$ [33], Therefore, only impurity scattering is not sufficient to understand the negative $\Delta\rho_0$ in the regime with weak impurity level.

Very recently, Sugimoto *et al.* tried to theoretically reproduce the sign-reversal of in-plane resistivity anisotropy in the AFM state based on the interplay of impurity scattering and the anisotropic electronic states of RFS [20]. The anisotropy was thought to be dominated by the non-Dirac electron Fermi pockets near the Γ point in the existence of impurity potential [20]. In their model, negative $\Delta\rho_0$ can be realized as the electron pockets disappear with increasing hole doping level [20]. However, there is no such experimental result for the evolution of the RFS in the hole-underdoped samples up to now. As a result, further experiments on these hole-underdoped crystals, such as ARPES and quantum oscillation, are required to examine the validity of the theoretical explanations.

No matter what is actually responsible for the sign reversal of $\Delta\rho$ deep inside the AFM state with increasing hole doping level, the intersection between $\rho_a(T)$ and $\rho_b(T)$ in $Ca_{0.81}Na_{0.19}Fe_2As_2$, with $\Delta\rho > 0$ in a short interval of temperature below T_N (110 K $< T <$ 165 K) while $\Delta\rho < 0$ deep inside the AFM state ($T <$ 110 K), cannot be simply attributed to a single mechanism but should be the result of a combined effect of different mechanisms. Apparently, $\Delta\rho$ in the temperatures of 110 K $< T <$ 165 K inherits the positive sign of $\Delta\rho$ above T_N, suggesting that the sign of anisotropy in this temperature region is still dominated by the magnetic scattering of spin fluctuation although spin fluctuation becomes weaker after entering the AFM state. Upon cooling from T_N to 110 K, the magnitude of $\Delta\rho$ continuously decreases in the sample with $x = 0.19$, indicating that the contributions from different mechanisms lead to different signs of $\Delta\rho$ and compete with each other below T_N in this doping level. However, in the other doping levels we investigate, the data shown in Fig. 6(a) suggest that the different mechanisms give the same signs of contributions to $\Delta\rho$. In one word, the complicated evolutions of resistivity anisotropy $\Delta\rho$ with hole doping level and temperature shown in Fig. 6(a) suggest cooperative effect of the contributions to $\Delta\rho$ from the different mechanisms: spin fluctuation, impurity scattering, and anisotropic electronic state of the RFS. These observations provide the hints to theoretical explanation of the in-plane resistivity anisotropy in the AFM state.

IV. CONCLUSION

In conclusion, we investigated the in-plane resistivity anisotropy in the detwinned hole-underdoped $Ca_{1-x}Na_xFe_2As_2$ single crystals and observed the sign reversal of in-plane resistivity anisotropy with increasing hole doping level from $x = 0.11$ and 0.14 to $x = 0.24$ and 0.30 in the detwinned hole-underdoped $Ca_{1-x}Na_xFe_2As_2$ single crystals and an intersection between $\rho_a(T)$ and $\rho_b(T)$ deep inside the AFM state for the crystal with $x = 0.19$. These results suggests that the anisotropic resistivity in the AFM state strongly depends on the competition of the contributions from different mechanisms. Such competition between the different mechanisms leads to the complicated evolution of the anisotropy of the in-plane resistivity with doping level.

ACKNOWLEDGMENTS

The authors would like to thank L. J. Zou, S. Y. Li, Z. Sun, Y. M. Xiong, and T. Wu for useful discussions. This work is supported by the National Natural Science Foundation of China (Grants No. 11190021, No. 11174266, and No. 91122034) and the "Strategic Priority Research Program (B)" of the Chinese Academy of Sciences (Grant No. XDB04040100), the National Basic Research Program of China (973 Program, Grant No. 2011CBA00101), Anhui Provincial Natural Science Foundation (Grant No. 1308085MA05), the Fundamental Research Funds for the Central Universities (Programs No. WK2030020020 and No. WK2340000035).

[1] Clarina de la Cruz, Q. Huang, J. W. Lynn, Jiying Li, W. Ratcliff II, J. L. Zarestky, H. A. Mook, G. F. Chen, J. L. Luo, N. L. Wang, and Pengcheng Dai, Nature (London) **453**, 899 (2008).

[2] J. H. Chu, J. G. Analytis, K. D. Greve, P. L. McMahon, Z. Islam, Y. Yamamoto, and I. R. Fisher, Science **329**, 824 (2010).

[3] H. H. Kuo, J. H. Chu, S. C. Riggs, L. Yu, P. L. McMahon, K. DeGreve, Y. Yamamoto, J. G. Analytis, and I. R. Fisher, Phys. Rev. B **84**, 054540 (2011).

[4] M. A. Tanatar, E. C. Blomberg, A. Kreyssig, M. G. Kim, N. Ni, A. Thaler, S. L. Budko, P. C. Canfield, A. I. Goldman, I. I. Mazin, and R. Prozorov, Phys. Rev. B **81**, 184508 (2010).

[5] J. J. Ying, X. F. Wang, T. Wu, Z. J. Xiang, R. H. Liu, Y. J. Yan, A. F. Wang, M. Zhang, G. J. Ye, P. Cheng, J. P. Hu, and X. H. Chen, Phys. Rev. Lett. **107**, 067001 (2011).

[6] S. Ishida, M. Nakajima, T. Liang, K. Kihou, C. H. Lee, A. Iyo, H. Eisaki, T. Kakeshita, Y. Tomioka, T. Ito, and S. Uchida, J. Am. Chem. Soc. **135**, 3158 (2013).

[7] R. M. Fernandes, E. Abrahams, and J. Schmalian, Phys. Rev. Lett. **107**, 217002 (2011).

[8] W. C. Lv and P. Phillips, Phys. Rev. B **84**, 174512 (2011).

[9] H. H. Kuo and I. R. Fisher, arXiv:1311.0933.

[10] M. Yi, D. H. Lu, J. H. Chu, J. G. Analytis, A. P. Sorini, A. F. Kemper, B. Moritz, S. K. Mo, R. G. Moore, M. Hashimoto, W. S. Lee, Z. Hussain, T. P. Devereaux, I. R. Fisher, and Z. X. Shen, Proc. Natl. Acad. Sci. U.S.A. **108**, 6878 (2011).

[11] T. M. Chuang, M. P. Allan, Jinho Lee, Yang Xie, Ni Ni, S. L. Budko, G. S. Boebinger, P. C. Canfield, and J. C. Davis, Science **327**, 181 (2010).

[12] M. P. Allan, T. M. Chuang, F. Massee, Yang Xie, Ni Ni, S. L. Budko, G. S. Boebinger, Q. Wang, D. S. Dessau, P. C. Canfield, M. S. Golden, and J. C. Davis, Nat. Phys. **9**, 220 (2013).
[13] A. Dusza, A. Lucarelli, F. Pfuner, J.-H. Chu, I. R. Fisher, and L. Degiorgi, Europhys. Lett. **93**, 37002 (2011).
[14] S. Kasahara, H. J. Shi, K. Hashimoto, S. Tonegawa, Y. Mizukami, T. Shibauchi, K. Sugimoto, T. Fukuda, T. Terashima, Andriy H. Nevidomskyy, and Y. Matsuda, Nature (London) **486**, 382 (2012).
[15] K. K. Huynh, Y. Tanabe, and K. Tanigaki, Phys. Rev. Lett. **106**, 217004 (2011).
[16] P. Richard, K. Nakayama, T. Sato, M. Neupane, Y.-M. Xu, J. H. Bowen, G. F. Chen, J. L. Luo, N. L. Wang, X. Dai, Z. Fang, H. Ding, and T. Takahashi, Phys. Rev. Lett. **104**, 137001 (2010).
[17] T. Terashima, N. Kurita, M. Tomita, K. Kihou, C. H. Lee, Y. Tomioka, T. Ito, A. Iyo, H. Eisaki, T. Liang, M. Nakajima, S. Ishida, S. I. Uchida, H. Harima, and S. Uji, Phys. Rev. Lett. **107**, 176402 (2011).
[18] T. Shimojima, K. Ishizaka, Y. Ishida, N. Katayama, K. Ohgushi, T. Kiss, M. Okawa, T. Togashi, X.-Y. Wang, C.-T. Chen, S. Watanabe, R. Kadota, T. Oguchi, A. Chainani, and S. Shin, Phys. Rev. Lett. **104**, 057002 (2010).
[19] Y. K. Kim, H. Oh, C. Kim, D. Song, W. Jung, B. Kim, H. J. Choi, C. Y. Kim, B. Lee, S. Khim, H. Kim, K. H. Kim, J. B. Hong, and Y. S. Kwon, Phys. Rev. B **83**, 064509 (2011).
[20] K. Sugimoto, P. Prelovsek, E. Kaneshita, and T. Tohyama, arXiv:1312.2322.
[21] B. Valenzuela, E. Bascones, and M. J. Calderon, Phys. Rev. Lett. **105**, 207202 (2010).
[22] S. Ishida, T. Liang, M. Nakajima, K. Kihou, C. H. Lee, A. Iyo, H. Eisaki, T. Kakeshita, T. Kida, M. Hagiwara, Y. Tomioka, T. Ito, and S. Uchida, Phys. Rev. B **84**, 184514 (2011).
[23] S. Ishida, M. Nakajima, T. Liang, K. Kihou, C. H. Lee, A. Iyo, H. Eisaki, T. Kakeshita, Y. Tomioka, T. Ito, and S. Uchida, Phys. Rev. Lett. **110**, 207001 (2013).
[24] E. C. Blomberg, M. A. Tanatar, R. M. Fernandes, I. I. Mazin, Bing Shen, Hai-Hu Wen, M. D. Johannes, J. Schmalian, and R. Prozorov, Nat. Commun. **4**, 1914 (2013).
[25] K. Zhao, Q. Q. Liu, X. C. Wang, Z. Deng, Y. X. Lv, J. L. Zhu, F. Y. Li, and C. Q. Jin, Phys. Rev. B **84**, 184534 (2011).
[26] H. Chen, Y. Ren, Y. Qiu, Wei Bao, R. H. Liu, G. Wu, T. Wu, Y. L. Xie, X. F. Wang, Q. Huang, and X. H. Chen, Europhys. Lett. **85**, 17006 (2009).
[27] M. A. Tanatar, A. Kreyssig, S. Nandi, N. Ni, S. L. Bud'ko, P. C. Canfield, A. I. Goldman, and R. Prozorov, Phys. Rev. B **79**, 180508(R) (2009).
[28] J. H. Chu, J. G. Analytis, D. Press, K. DeGreve, T. D. Ladd, Y. Yamamoto, and I. R. Fisher, Phys. Rev. B **81**, 214502 (2010).
[29] Y. Xiao, Y. Su, W. Schmidt, K. Schmalzl, C. M. N. Kumar, S. Price, T. Chatterji, R. Mittal, L. J. Chang, S. Nandi, N. Kumar, S. K. Dhar, A. Thamizhavel, and Th. Brueckel, Phys. Rev. B **81**, 220406(R) (2010).
[30] I. R. Fisher, L. Degiorgi, and Z. X. Shen, Rep. Prog. Phys. **74**, 124506 (2011).
[31] Y. Mizuguchi, Y. Hara, K. Deguchi, S. Tsuda, T. Yamaguchi, K. Takeda, H. Kotegawa, H. Tou, and Y. Takano, Supercond. Sci. Technol. **23**, 054013 (2010).
[32] S. H. Liang, G. Alvarez, C. Sen, A. Moreo, and E. Dagotto, Phys. Rev. Lett. **109**, 047001 (2012).
[33] Y. J. Yan, A. F. Wang, X. G. Luo, Z. Sun, J. J. Ying, G. J. Ye, P. Chen, J. Q. Ma, and X. H. Chen, arXiv:1301.1734.